Seventh International Conference on Computational Fluid Dynamics (ICCFD7), Big Island, Hawaii, July 9-13, 2012

ICCFD7-1106

Stability and transition in the near-field of pure thermal planar plumes

T. Hattori*, S. W. Armfield*, M. P. Kirkpatrick* and S. E. Norris**
Corresponding author: tae.hattori@sydney.edu.au

* School of Aerospace, Mechanical and Mechatronic Engineering, The University of Sydney, Sydney, NSW 2006, Australia
** Mechanical Engineering, The University of Auckland, Auckland, New Zealand

Abstract: The near-field of a buoyant plume exhibits puffing behaviour characterised by the periodic formation of vortical structures (puffs). In this study, a plume is generated from a finite-width fixed temperature planar source. The periodic formation of puffs is seen to be associated with an instability in the thermal boundary layer that forms on the heated source region away from the plume axis. The instability produces a bulge in the thermal boundary layer, that is further investigated by modelling the boundary layer flow in the vicinity of the plume source by use of a channel flow with a heated floor section.

Keywords: Natural Convection, Direct Numerical Simulation

1 Introduction

The near-field behaviour of a buoyant plume in the transitional regime is characterised by the periodic formation of vortical structures (puffing). Such behaviour has been observed for forced axisymmetric plumes [1, 2, 3, 4], for forced planar plumes [5, 6], for a pure thermal axisymmetric plume [7] and for a pure thermal planar plume recently by Hattori et al. [8]. Similar plume behaviour has also been observed in the transitional ventilated filling box flow with a line heat source in Hattori et al. [9].

Plourde et al. [7] observed for a pure thermal axisymmetric plume the puffing is associated with an instability of the lapping flow, which develops on the heated source region on either side of the plume axis, forming a thermal plumelet (bulge), that eventually merges with and surrounds the central ascending column. We also observed for a pure thermal planar plume the bulge forming and its growth along the lapping flow, which eventually surrounds the central column, in the present study and in our recent study [8], which provided experimental validation for the near-field unsteady behaviour that is numerically investigated.

We will focus on the near-field plume instability, namely the bulge forming in the lapping flow, and the associated puffing behaviour. The formation of the bulge and its dependence on the lapping flow velocity along the bottom boundary are further investigated by modelling the boundary layer flow in the vicinity of the plume source by a channel flow with a heated floor section, providing an additional control parameter. Three dimensional direct numerical simulations are used to obtain the near-field planar plume flow and the channel flow, both with Prandtl number of 7.0 and Reynolds numbers in the range $200 \leq \mathrm{Re} \leq 1000$. Three-dimensional effects were found to be small in this flow for the range of Re considered.

2 Problem definition

The computational domains are shown in Figures 1a and 1b for the planar plume and the channel flow with a heated floor section, respectively. A channel height of 0.5 is used. The governing equations are the

non-dimensional, incompressible Navier-Stokes equations with the Boussinesq approximation for buoyancy.

$$\frac{\partial u_i}{\partial t} + \frac{\partial \left(u_j u_i\right)}{\partial x_j} = -\frac{dp}{dx_i} + \frac{\partial}{\partial x_j}\left(\frac{1}{\mathrm{Re}}\frac{\partial u_i}{\partial x_j}\right) + T\delta_{i2}, \tag{1}$$

$$\frac{\partial T}{\partial t} + \frac{\partial \left(u_i T\right)}{\partial x_i} = \frac{\partial}{\partial x_i}\left(\frac{1}{\mathrm{Re}\,\mathrm{Pr}}\frac{\partial T}{\partial x_i}\right), \tag{2}$$

$$\frac{\partial u_i}{\partial x_i} = 0, \tag{3}$$

where $i = 1, 2, 3$ and $j = 1, 2, 3$. $x_1 = x$, $x_2 = y$ and $x_3 = z$ are the coordinates as shown in Figures 1a and 1b, and t is time. $u_1 = u$, $u_2 = v$ and $u_3 = w$ are the velocity components in the x, y and z directions, respectively. p is the pressure perturbation and T the temperature perturbation given as $T = \left(T^* - T^*_\infty\right)/\left(T^*_s - T^*_\infty\right)$, where T^* is the dimensional local temperature, T^*_∞ the dimensional ambient temperature and T^*_s the dimensional source temperature. The superscript, $*$, is used for dimensional quantities.

Control parameters for the plume are the Reynolds and Prandtl numbers. The Reynolds number is defined as $\mathrm{Re} = U^* L^*/\nu^*$, where $U^* = \sqrt{g^*\beta^*(T^*_s - T^*_\infty)L^*}$, with L^* the plume source width, ν^* the kinematic viscosity, g^* the gravitational acceleration, and β^* is the thermal expansion coefficient. The Prandtl number is $\mathrm{Pr} = \nu^*/\kappa^*$, with κ^* the thermal diffusivity. In the case of the channel flow with a heated floor section, in addition to the above two parameters, the inlet velocity (u_{in}) is controlled to vary a Froude number, defined as $\mathrm{Fr} = U^*_{\delta^*_T}/U^*$, where $U^*_{\delta^*_T}$ is the average horizontal velocity in the thermal boundary layer, of thickness δ^*_T, obtained as $U^*_{\delta^*_T} = \int_0^{\delta^*_T}\langle u^*\rangle dy^*/\delta^*_T$, with $\langle\rangle$ the time averaging operator.

3 Numerical method

For the study, a non-staggered, Cartesian mesh, finite volume code [10], written in the FORTRAN90 language, was used . The code is based on a fractional step method (the $P2$ pressure correction method) [11], with the Adams-Bashforth and Crank-Nicolson time discretisation schemes being used for the advection and diffusion terms, respectively. In the code, the transport equations (Equations (1) and (2)), discretised in the forms below, were solved for $u_i^\dagger$, a velocity estimate, and T^{n+1}, respectively (the following discretisations are based on a constant time stepping size, Δt):

$$\frac{u_i^\dagger - u_i^n}{\Delta t} + \frac{3}{2}A\left(u_i^n\right) - \frac{1}{2}A\left(u_i^{n-1}\right) = -G\left(p^n\right) + \frac{1}{2\,\mathrm{Re}}L\left(u_i^\dagger + u_i^n\right), \tag{4}$$

and

$$\frac{T^{n+1} - T^n}{\Delta t} + \frac{3}{2}A\left(T^n\right) - \frac{1}{2}A\left(T^{n-1}\right) = \frac{1}{2\,\mathrm{Re}\,\mathrm{Pr}}L\left(T^{n+1} + T^n\right), \tag{5}$$

where A is the discrete advection operator, G the discrete gradient, L the discrete Laplace operator, and the superscripts, n and $n+1$, are the previous and current time steps, respectively. The Poisson pressure correction equation was discretised in the form:

$$\Delta t L\left(pc\right) = D\left(u_i^\dagger\right), \tag{6}$$

where pc is the pressure correction term with D the discrete divergence, and was solved for pc. A divergence-free velocity field is then obtained by correcting velocities with:

$$u_i^{n+1} = u_i^\dagger - \Delta t G\left(pc\right). \tag{7}$$

The cell face values for velocity required in the right hand side of Equation (6) and for the advection velocities in Equations (1) and (2) or (4) and (5) were interpolated using Rhie-Chow interpolation method [12] in order to avoid checkerboarding in the pressure field, where pressures on odd and even nodes are uncoupled.

The spatial discretisations for the diffusion terms in Equations (1) and (2) used second-order central

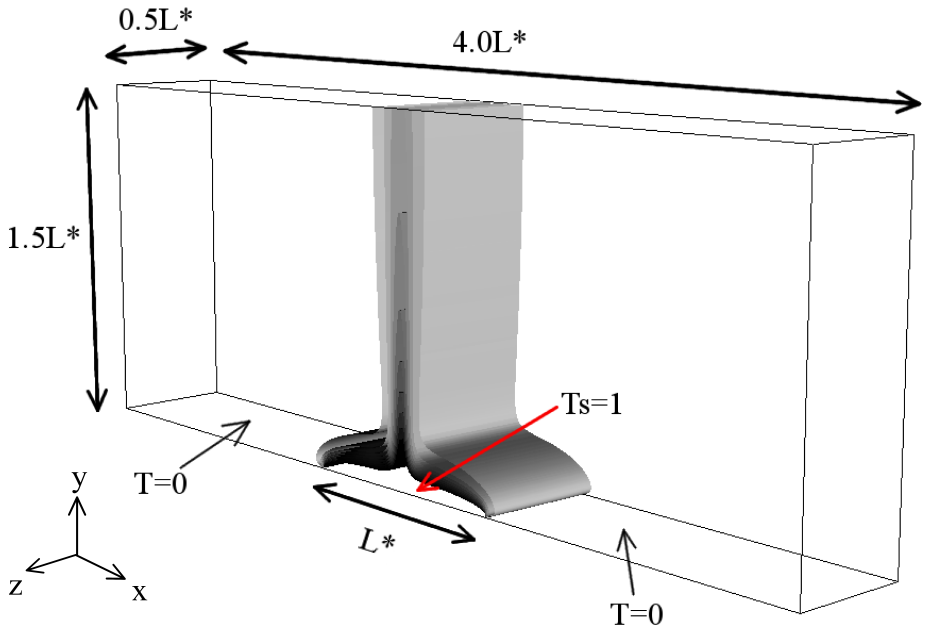

(a) Plume flow

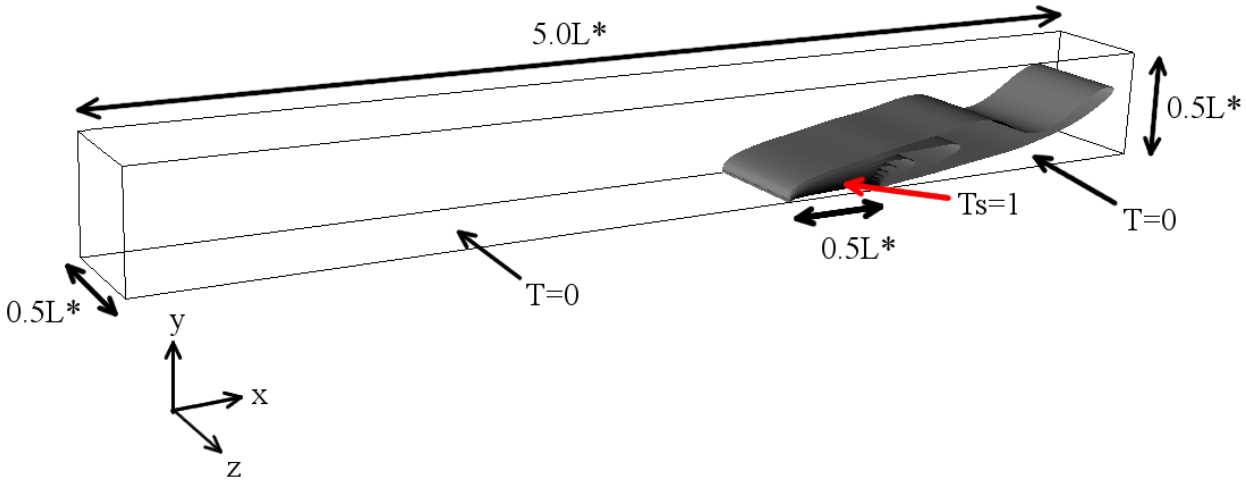

(b) Chanel flow

Figure 1: Computational domains for the plume flow and the channel flow with a heated floor section

differencing. The spatial discretisations for the advection terms in Equation (1) used second-order central differencing, while those in Equation (2) used fourth-order central differencing with the ULTRA (Universal Limiter for Tight Resolution and Accuracy) flux limiter [13] in order to avoid instability due to a large cell Peclet number, $\mathrm{Pe} = u_i \Delta x_i \,\mathrm{Re}\,\mathrm{Pr}$.

The Strongly Implicit Procedure (SIP) [14] was used for Equations (1) and (2), and the Bi-Conjugate Gradient Stabilised method (BICGSTAB) [15] using a SIP preconditioner was used for the Poisson pressure correction equation. Using the $P2$ pressure correction method [11], the solver is computationally efficient, with each of Equations (1) and (2) and the Poisson pressure correction equation, being solved only once per time step. Convergence criteria were applied to ensure that the divergence was kept below $\sim 1.0 \times 10^{-10}$ at each time step. For both the plume and channel flows, the time step, Δt, was varied to maintain the Courant number ($= u_i \Delta t / \Delta x_i$) within the range $0.15 - 0.3$.

For the plume flow, the following boundary conditions were imposed:

- The bottom boundary is a rigid, no-slip wall, where all the velocity components are zero. The thermal source in the region $-0.5 \leq x \leq 0.5$ is maintained at $T = 1$, and the rest of the bottom boundary is maintained at $T = 0$. For the pressure correction, a Neumann condition with zero normal derivative is applied. The pressure perturbation, p, on the external node is obtained by a second order extrapolation from the interior.

- At the x boundaries, a Neumann condition with zero normal derivative is applied for the normal velocity component, u, and the tangential velocities, v and w, are zero. The temperature perturbation, T, is set to zero for inflows, while a Neumann condition with zero normal derivative is applied for outflow temperatures. Both p and the pressure correction are zero.

- At the top boundary, a Neumann condition with zero normal derivative is applied for all the velocity components and T, with the normal velocity component, v, only taking a positive value, i.e. no inflow is allowed. Both p and the pressure correction are zero.

- The periodic condition is employed for the z boundaries.

For the channel flow with a heated floor section, the following boundary conditions were imposed:

- The bottom boundary is a rigid, no-slip wall, where all the velocity components are zero. The heated floor section $3.0 \leq x \leq 3.5$ is maintained at $T = 1$, and the rest of the bottom boundary is maintained at $T = 0$. For the pressure correction, a Neumann condition with zero normal derivative is applied, and p on the external node is obtained by a second order extrapolation.

- The top boundary is a slip plane where a Neumann condition with zero normal derivative is applied for the tangential velocities, u and w, and T, while the normal velocity component, v, is zero. For the pressure correction, a Neumann condition with zero normal derivative is applied, and p on the external node is obtained by a second order extrapolation.

- At the left inlet boundary, the normal velocity component, u, is set to a constant velocity, u_{in}, while the tangential velocities, v and w, are zero. T is set to zero. For the pressure correction, a Neumann condition with zero normal derivative is applied, and p on the external node is obtained by a second order extrapolation.

- At the right outlet boundary, a Neumann condition with zero normal derivative is applied for all the velocity components and T, with the normal velocity component, u, only taking a positive value, i.e. no inflow is allowed. Both p and the pressure correction are zero.

- The periodic condition is employed for the z boundaries.

For the plume flow, a uniform grid was used both in the y and z directions, while for the discretisation in the x direction a uniform grid was used in the region $-1.0 \leq x \leq 1.0$ and a nonuniform grid with one percent linear stretching was used in the regions $x < -1.0$ and $x > 1.0$. The effects of the grid size, the domain size and the time for calculating statistics on the solution accuracies were examined for the case with $\mathrm{Re} = 1000$. It was found that statistical solutions obtained with the domain size of $X \times Y \times Z =$

$4.0 \times 1.5 \times 0.5$ over the time, $t = 40 - 100$, show negligible variations with respect to those obtained with extended domain sizes and longer times for statistics calculation. It was further found that using the grid size, $\Delta x \times \Delta y \times \Delta z = 0.01 \times 0.0063 \times 0.01$ (in the region of a uniform grid), with the number of grid points, $N_x \times N_y \times N_z = 338 \times 240 \times 50$, both the statistical and transient solutions show a negligible grid dependency. Three-dimensional effects were shown to be small, with the magnitude of w typically below 1.0×10^{-3} for $\mathrm{Re} = 1000$ (in comparison, the magnitudes of u and v are in the order of 10^{-1}), and it reduces with reducing Re.

For the channel flow with a heated floor section, a uniform grid was used in all directions. As with the plume flow, the effects of the grid size, the domain size and the time for calculating statistics on the solution accuracies were examined for the case with $\mathrm{Re} = 1000$ and $u_{in} = 0.1$. For the examination of the domain size dependency, the domain sizes in the x and z directions were varied, while the domain size in the y direction, i.e. the channel height, was fixed at $y = 0.5$. It was found that statistical solutions obtained with the domain size of $X \times Y \times Z = 5.0 \times 0.5 \times 0.5$, over the time, $t = 40 - 100$, show negligible variations with respect to those obtained with extended domain sizes and longer times for statistics calculation. Further, using the grid size, $\Delta x \times \Delta y \times \Delta z = 0.02 \times 0.0083 \times 0.025$, with the number of grid points, $N_x \times N_y \times N_z = 250 \times 60 \times 20$, both the statistical and transient solutions were found to show a negligible grid dependency.

4 Results

4.1 Bulge forming instability and its parametric dependence

The instantaneous temperature fields are shown for cases with and without the bulge formation for the plume and channel flows in Figures 2 and 3, respectively. The lapping flow develops over the heated region. The red arrows are shown to indicate the directions of the lapping flow velocity. For plumes, the heated fluid in the lapping flow flows towards the central axis due to the entrainment by the central column. Figures 2b and 3b show the formation of bulges along the lapping flow. In Figure 2b, the formation of a puff along the plume axis is also shown. It is observed in both flows that the thickness of the thermal boundary layer is thinner for the higher Re, therefore it is considered that at a higher Re the Rayleigh-Taylor fluid layer is more sensitive to a small perturbation and hence is more likely to form the instability bulges.

The Froude number is defined as $\mathrm{Fr} = U^*_{\delta^*_T}/U^*$ with $U^*_{\delta^*_T} = \int_0^{\delta^*_T} \langle u^* \rangle dy^*/\delta^*_T$ in Section 2. In terms of non-dimensional quantities, it reduces to:

$$\mathrm{Fr} = \int_0^{\delta_T} \langle u \rangle dy/\delta_T, \tag{8}$$

where δ_T is the non-dimensional thickness of the thermal boundary layer. We define δ_T as the vertical distance measured from the bottom boundary to the location where the mean temperature, averaged in the z direction, $\langle T \rangle$, reduces to 0.01, at the location, 0.1 downstream of the beginning of the heated region, i.e. $x = \pm 0.4$ for the plume flow and $x = 3.1$ for the channel flow. For the plume flow, the vertical profiles of $\langle T \rangle$ and the mean horizontal velocity, averaged in the z direction, $\langle u \rangle$, at the locations, $x = \pm 0.4$, were averaged. For both the plume and channel flows, Fr was then calculated using Equation (8) at the location, 0.1 downstream of the beginning of the heated region. The values of Fr obtained in this way are shown in Tables 1 and 2 for the plume and channel flows, respectively.

In order to obtain a scaling relation for the mean thickness of the lapping flow thermal boundary layer, the balance equation for temperature is considered. For the mean lapping flow, adjacent to the bottom heated section, the horizontal advection term dominates, and the vertical and spanwise advection terms are considered to be small. Further, the vertical diffusion term dominates, and the horizontal and spanwise diffusion terms are considered to be small. Hence, Equation (2) reduces to:

$$\frac{\partial \langle uT \rangle}{\partial x} \approx \frac{1}{\mathrm{Re}\,\mathrm{Pr}} \frac{\partial^2 \langle T \rangle}{\partial^2 y}. \tag{9}$$

Further,

$$\frac{\langle u\rangle\langle T\rangle}{x} \sim \frac{1}{\mathrm{Re}\,\mathrm{Pr}}\frac{\langle T\rangle}{y^2}. \tag{10}$$

Therefore, at a fixed horizontal location, the thickness of the thermal boundary layer scales as:

$$\delta_T \sim \frac{1}{\langle u_{advec}\rangle^{\frac{1}{2}}\,\mathrm{Re}^{\frac{1}{2}}\,\mathrm{Pr}^{\frac{1}{2}}}, \tag{11}$$

where $\langle u_{advec}\rangle$ is the mean horizontal advection velocity, which may be assumed to be the average horizontal velocity in the lapping flow thermal boundary layer, that is $\mathrm{Fr} = \int_0^{\delta_T}\langle u\rangle dy/\delta_T$, hence:

$$\delta_T \sim \frac{1}{\mathrm{Re}^{\frac{1}{2}}\,\mathrm{Pr}^{\frac{1}{2}}\,\mathrm{Fr}^{\frac{1}{2}}}. \tag{12}$$

This is consistent with the correlation given in Fujii [16], i.e. $\delta_T \sim 1/\,\mathrm{Pr}^{\frac{1}{2}}$, and also with Figures 2 and 3 both showing a reduction in δ_T with an increase in Re. From Equation (12), for a fixed Pr, $\delta_T \sim 1/\left(\mathrm{Re}^{\frac{1}{2}}\,\mathrm{Fr}^{\frac{1}{2}}\right)$. The average of $\langle T\rangle$ at $x = \pm 0.4$ is plotted over the normalised height, $y\,\mathrm{Re}^{\frac{1}{2}}\,\mathrm{Fr}^{\frac{1}{2}}$, for the plume flow with different Re in Figure 4, and $\langle T\rangle$ at $x = 3.1$ for the channel flow with different Re and u_{in} in Figure 5. It is shown that $\langle T\rangle$ falls onto a single curve in both cases, which validates the scaling relation obtained above.

Figure 6 contains a mapping of bulge formation against Re and Fr for the results shown in Tables 1 and 2. The formations of the bulges for both the plume and channel flows, and the puffs for the plume flow, have been examined by studying the flow animations for each case. For the channel flow, the bulge formation is shown to depend on Re and Fr. For the plume flow, the formation of puffs along the plume axis has been observed to be associated with the formation of bulges in the lapping flow, and the formation of bulges and puffs is shown to depend on Re. For the channel flow, the critical Re lies in the range $400 < \mathrm{Re} < 500$ and the critical Fr lies in the range $0.045 < \mathrm{Fr} < 0.05$, with the bulge observed above the critical Re and below the critical Fr. Further, it has been observed that at $\mathrm{Re} \geq 500$, the bulge forms for low enough Fr, while with increasing Fr (by increasing u_{in}) the bulge formation reduces and the flow eventually becomes steady. For the plume flow, the critical Re lies in the range $300 < \mathrm{Re} < 400$, with the bulge and puff observed above the critical Re. The results obtained for the plume and channel flows shown in Figure 6 are approximately consistent, indicating that the use of the channel flow model to study the lapping flow instability in the vicinity of the plume source is appropriate. The results above clearly show that the bulge formation along the lapping flow is dependent on both Re and Fr. It is further considered that one mechanism causing the Re dependence of the bulge formation is the Re dependence of the thermal boundary layer thickness, as shown by Equation (12) and the results in Figures 4 and 5. In the present cases where Pr is constant and the Fr variation is much smaller, compared to the Re variation, the Re variation is the dominant factor determining δ_T.

In order to examine the correlation between the location of the bulge formation and Fr, it is considered to be reasonable to use the location of the peak in the horizontal distribution of the mean buoyancy fluctuation, $\langle v'T'\rangle$, in the thermal boundary layer as a measure of the mean location of the bulge formation. Hence, for the cases where the bulge was found to form, the horizontal location of the peak in $\langle v'T'\rangle$ at $y\,\mathrm{Re}^{\frac{1}{2}}\,\mathrm{Fr}^{\frac{1}{2}} = 0.2$, measured from the beginning of the heated section, is plotted against Fr in Figure 7. Again, $\langle v'T'\rangle$ has been averaged in the z direction for both the plume and channel flows, and for the plume flow the $\langle v'T'\rangle$ profiles on either side of the line of symmetry, $x = 0.0$, have been averaged to obtain a single peak location for each case. As can be seen, the location of the peak in $\langle v'T'\rangle$ has a positive correlation with Fr, demonstrating that the bulge forms further downstream with increasing Fr. From this, it may be assumed that an increase in Fr reduces the spatial growth rate of the Rayleigh-Taylor instability, hence shifting the location of the bulge formation further downstream.

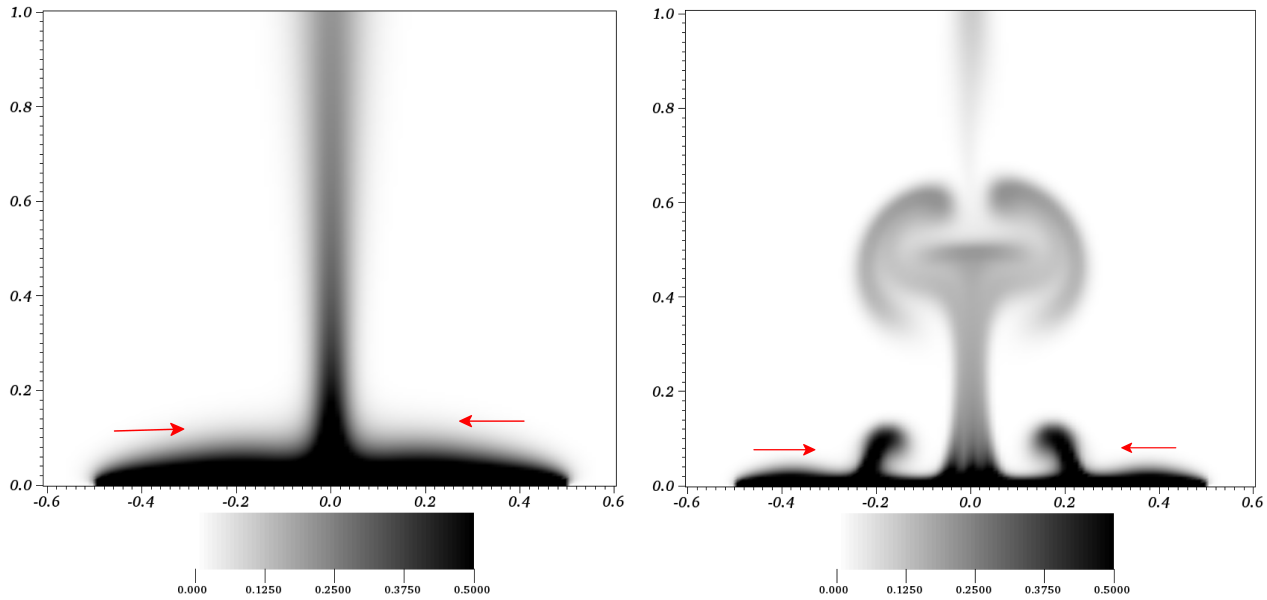

(a) Re = 300 (b) Re = 1000

Figure 2: Temperature fields for the plume flow ($t = 98$). The red arrows show the directions of the lapping flow velocity.

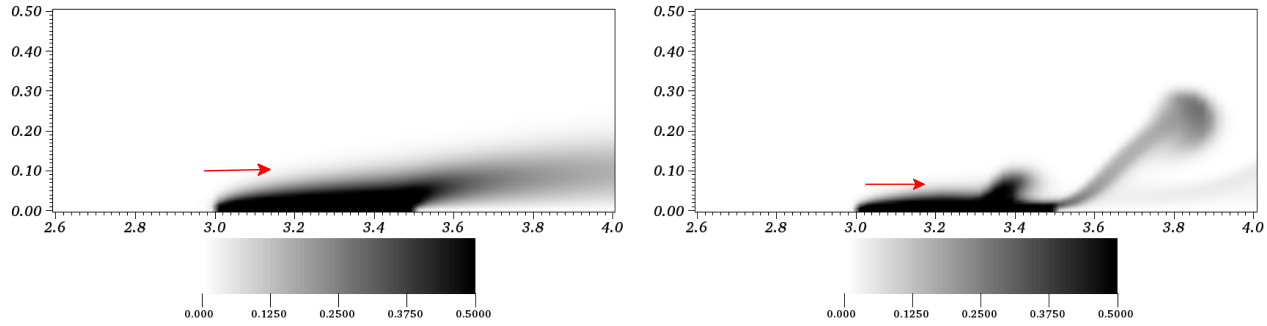

(a) Re = 400, Fr = 0.05508 (b) Re = 1000, Fr = 0.04523

Figure 3: Temperature fields for the channel flow ($t = 100$). The red arrows show the directions of the lapping flow velocity.

Table 1: Fr calculated for the plume flow with various Re

Re	**Fr**
200	0.04673
300	0.04077
400	0.03982
500	0.03956
600	0.03907
700	0.03796
800	0.03790
900	0.03750
1000	0.03714

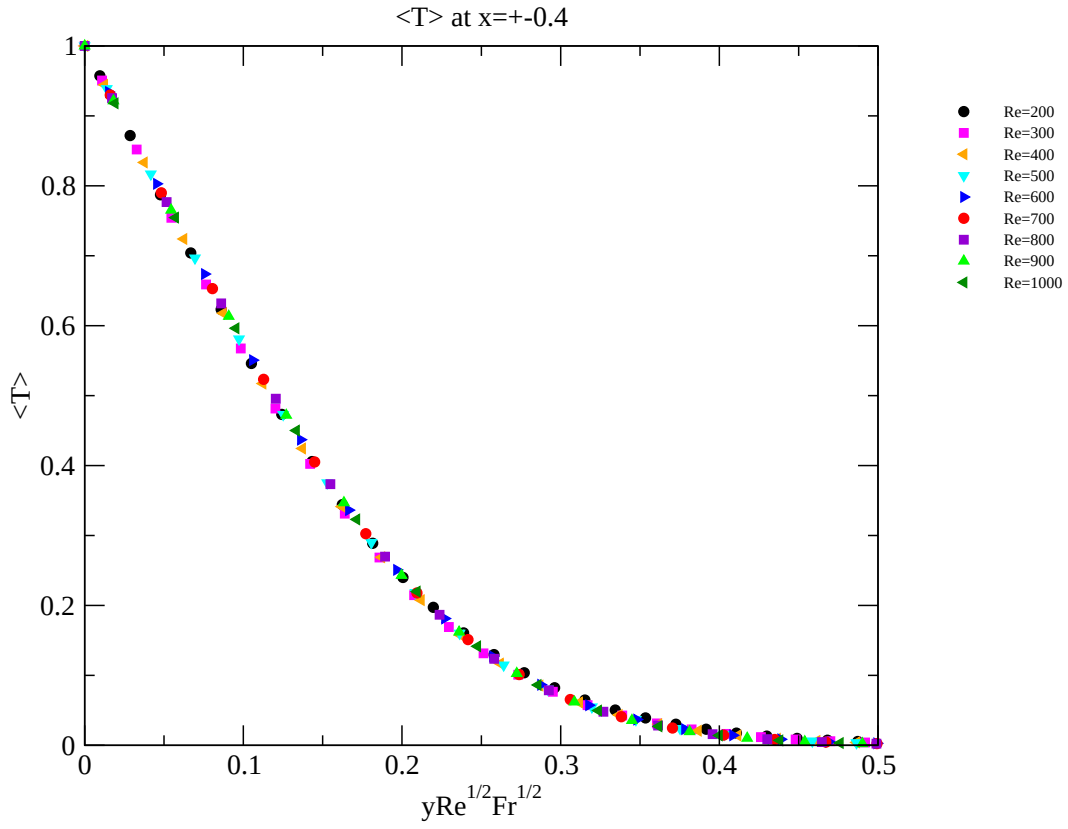

Figure 4: Mean temperature, $\langle T \rangle$, at $x = \pm 0.4$ over normalised height for the plume flow with various Re

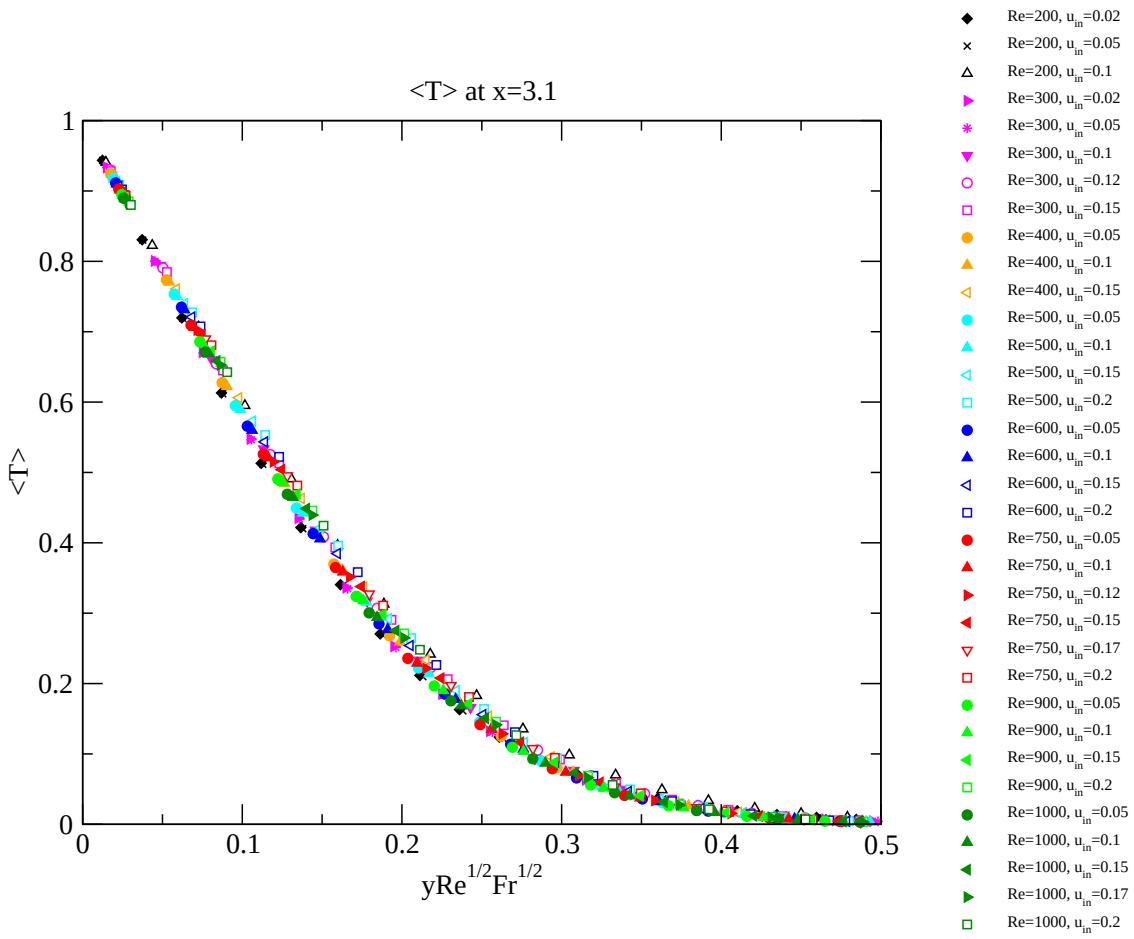

Figure 5: Mean temperature, $\langle T \rangle$, at $x = 3.1$ over normalised height for the channel flow with a heated floor section with various Re and u_{in}

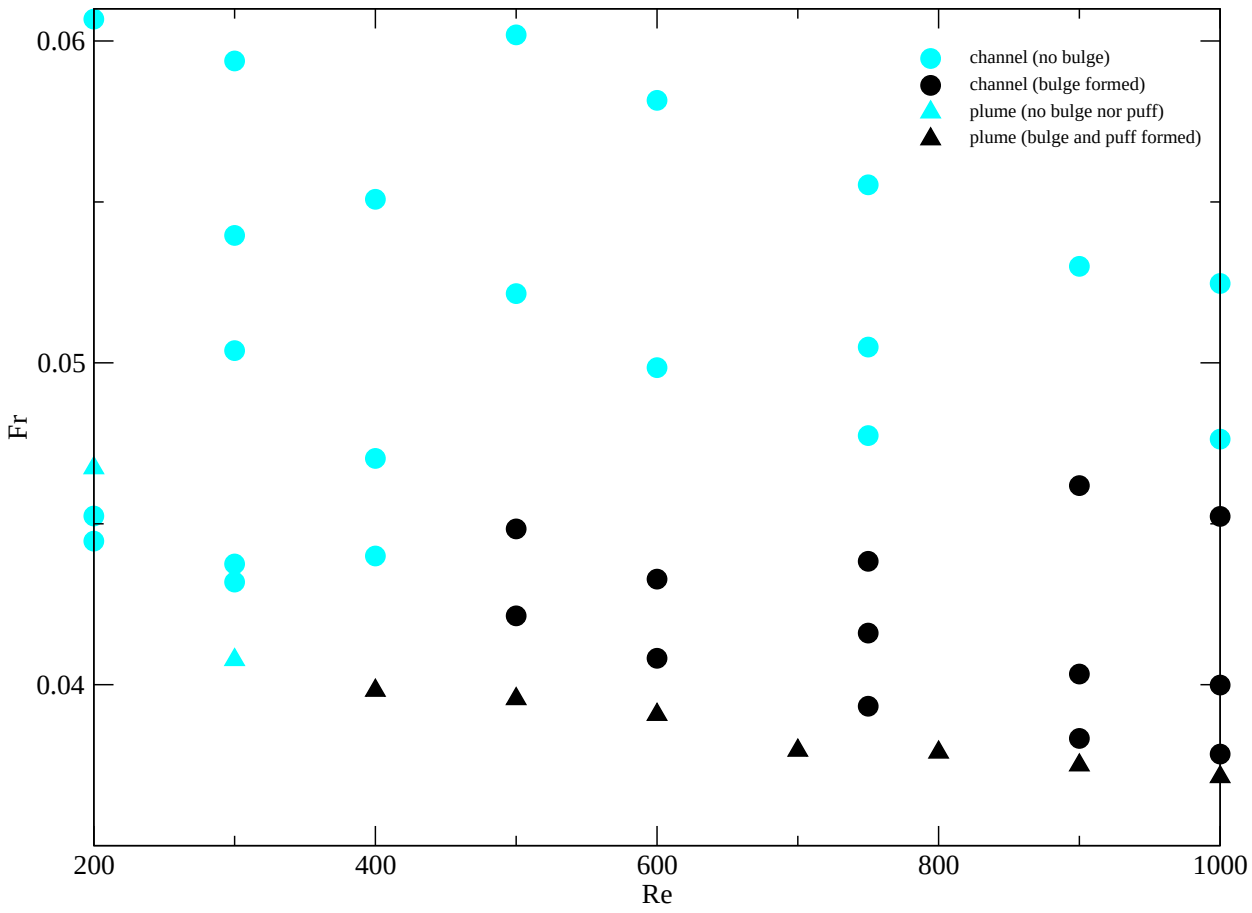

Figure 6: Mapping for the formations of the bulges in the lapping flow for both the plume and channel flows, and the puffs for the plume flow

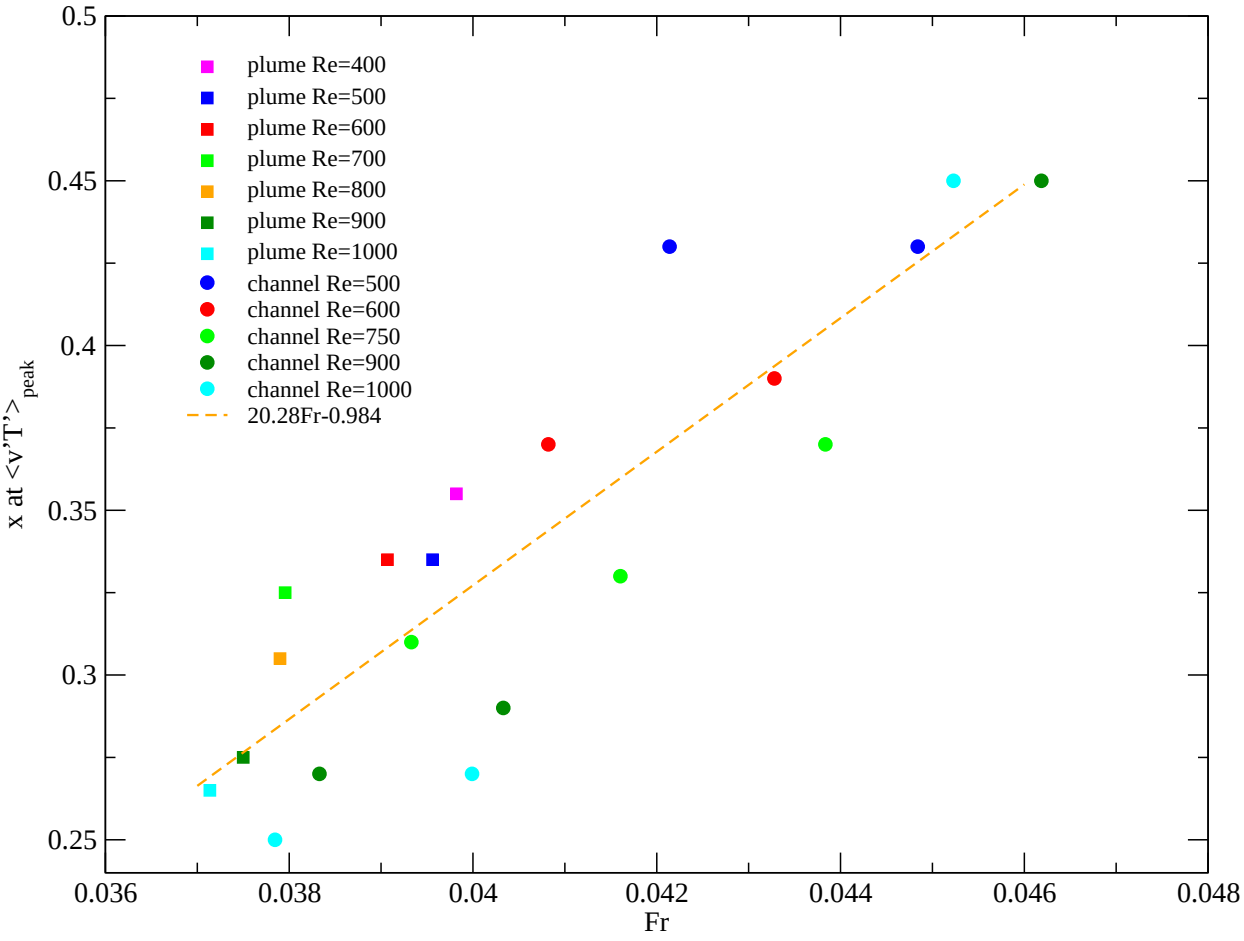

Figure 7: The correlation between the location of the bulge formation and Fr

4.2 Parametric dependence of oscillation frequencies

For the cases where the bulge was found to form, the non-dimensional oscillation frequencies (St) were determined by obtaining the temperature, T, as a function of time at particular locations and then performing a discrete Fourier transform on the signal. For the plume flow, T was obtained over 50 non-dimensional time units after the initial integration to $t = 100$ at the locations along the lapping flow, $(x, y, z) = (-0.25, 0.05, 0.0)$, $(-0.225, 0.05, 0.0)$, $(-0.2, 0.05, 0.0)$, $(-0.175, 0.05, 0.0)$ and $(-0.15, 0.05, 0.0)$, and along the plume axis, $(x, y, z) = (0.0, 0.1, 0.0)$ and $(0.0, 0.2, 0.0)$. For the channel flow, T was obtained over 50 non-dimensional time units after the initial integration to $t = 50$ at the location in the lapping flow, $(x, y, z) = (3.25, 0.05, 0.0)$.

From the plume results, it was found that the dominant frequencies at the different locations in the lapping flow are in excellent agreement for each Re and that the dominant frequency in the lapping flow, and its sub- and super-harmonics, are also dominating the oscillations at the locations along the plume axis, which suggests the existence of a convective-type instability of the near-field plume flow. For example, for the Re = 1000 case, the dominant oscillation frequency in the lapping flow was found to be St ≈ 0.24, with its sub-harmonic found at St ≈ 0.12 and its super-harmonics found at St ≈ 0.36, St ≈ 0.48 and St ≈ 0.6, and these frequencies were shown to be also dominating the oscillations along the plume axis.

From the channel flow results, it was found that at a constant Re, with increasing Fr the dominant frequency increases. Also with increasing Fr at a constant Re, there were shown to be a transition from a quasi-periodic to almost periodic mode, and a reduction in the amplitude at the dominant frequency. For example, for the flow with Re = 900, increasing Fr from 0.04033 to 0.04619 leads to an increase in the dominant frequency from St ≈ 0.24 to St ≈ 0.3 and a reduction in the amplitude at the dominant frequency from ≈ 0.23 to ≈ 0.016. This is consistent with the assumption made previously that an increase in Fr reduces the spatial growth rate of the Rayleigh-Taylor instability.

The dominant frequency in the lapping flow was seen to vary with Re for the plume flow, and for the channel flow the dominant frequency was seen to vary with both Re and Fr. In Figure 8, the dominant frequency, St_d, normalised by $\mathrm{Re}^{\frac{1}{2}}$, is plotted against Fr, shown in Tables 1 and 2, for both the plume and channel flows. It is shown that for all the plume flows and for the channel flows with $\mathrm{Fr} \lesssim 0.042$, $\mathrm{St}_d \,/\, \mathrm{Re}^{\frac{1}{2}}$ approximately follows the relationship, $\mathrm{St}_d \,/\, \mathrm{Re}^{\frac{1}{2}} = 0.3044\,\mathrm{Fr} - 0.00396$, while for the channel flows with $\mathrm{Fr} \gtrsim 0.043$, $\mathrm{St}_d \,/\, \mathrm{Re}^{\frac{1}{2}}$ approximately follows $\mathrm{St}_d \,/\, \mathrm{Re}^{\frac{1}{2}} = 0.4285\,\mathrm{Fr} - 0.00970$. This transition in the Fr dependence of the dominant oscillation frequency, with increasing Fr above Fr ≈ 0.043, may be associated with the transition from a quasi-periodic to periodic mode, although a clear mechanism is not known yet.

5 Conclusions

The near-field instability of the planar pure plume flow with $\mathrm{Re} = 200 - 1000$ and Pr = 7.0 was investigated using three-dimensional direct numerical simulations. The near-field plume flow is characterised by the puffing behaviour, the formation of vortical structures above the plume source. The puffing appears to be associated with the lapping flow instability, forming a bulge on either side of the plume axis. The formation of the bulge and its dependence on the lapping flow velocity were investigated by modelling the boundary layer flow adjacent to the plume source by a channel flow with a heated floor section, providing an additional control parameter, u_{in}, that is to vary Fr.

The study obtained approximately consistent results for both the plume and channel flows, indicating that the use of the channel flow model to study the lapping flow instability in the vicinity of the plume source is appropriate. The bulge forms above a critical Re and below a critical Fr. For the plume flow, the critical Re was found in the range $300 < \mathrm{Re} < 400$. For the channel flow, the critical Re was found in the range $400 < \mathrm{Re} < 500$ and the critical Fr in the range $0.045 < \mathrm{Fr} < 0.05$. The Re dependence of the bulge formation is considered to be at least partly due to the Re dependence of the thermal boundary layer thickness. The location of the bulge formation shows a positive correlation with Fr, hence a bulge forms

Table 2: Fr calculated for the channel flow with various Re and u_{in}

Re	$\boldsymbol{u_{in}}$	**Fr**
200	0.02	0.04446
200	0.05	0.04524
200	0.1	0.06068
300	0.02	0.04319
300	0.05	0.04375
300	0.1	0.05038
300	0.12	0.05396
300	0.15	0.05938
400	0.05	0.04400
400	0.1	0.04703
400	0.15	0.05508
500	0.05	0.04214
500	0.1	0.04484
500	0.15	0.05215
500	0.2	0.06019
600	0.05	0.04082
600	0.1	0.04328
600	0.15	0.04985
600	0.2	0.05816
750	0.05	0.03933
750	0.1	0.04160
750	0.12	0.04384
750	0.15	0.04774
750	0.17	0.05049
750	0.2	0.05553
900	0.05	0.03833
900	0.1	0.04033
900	0.15	0.04619
900	0.2	0.05300
1000	0.05	0.03785
1000	0.1	0.03999
1000	0.15	0.04523
1000	0.17	0.04763
1000	0.2	0.05247

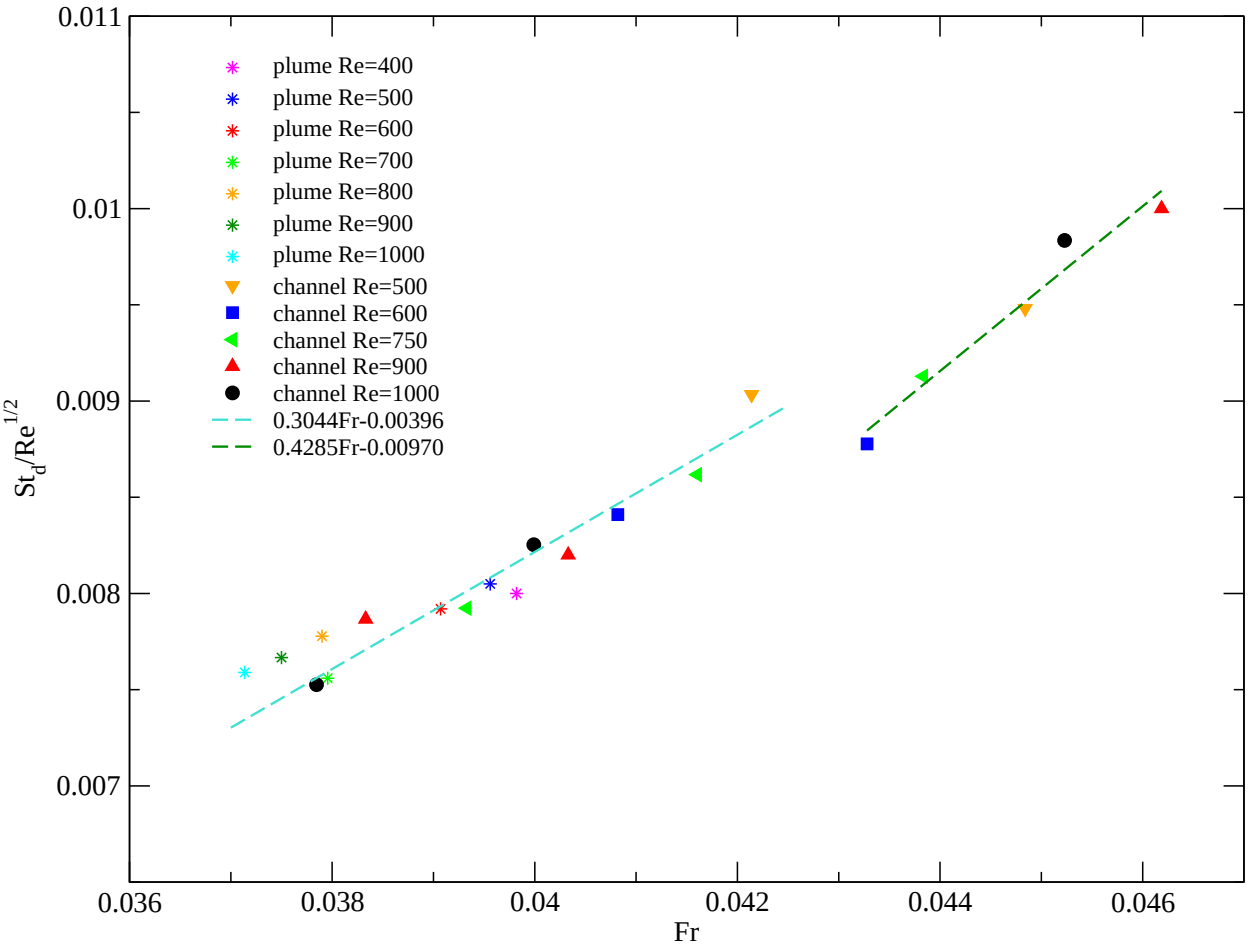

Figure 8: The dominant St_d in the lapping flow, normalised by $\mathrm{Re}^{\frac{1}{2}}$, plotted against Fr for both the plume and channel flows

further downstream with increasing Fr. It is therefore assumed that an increase in Fr reduces the spatial growth rate of the Rayleigh-Taylor instability.

The oscillation frequencies on the plume axis were found to be closely related to those in the lapping flow, which suggests the existence of a convective-type instability of the near-field plume flow. With increasing Fr for the channel flow at a constant Re, the flow undergoes a transition from a quasi-periodic to almost periodic mode, with a reduction in the amplitude at the dominant frequency. This also supports the assumption that an increase in Fr reduces the spatial growth rate of the Rayleigh-Taylor instability. Further, the dominant frequency in the lapping flow, for both the plume and channel flows, was found to scale with $\mathrm{Re}^{\frac{1}{2}}$ and Fr.

6 Acknowledgement

The authors gratefully acknowledge the support of the Australian Research Council.

References

[1] B. M. Cetegen and K. D. Kasper. Experiments on the oscillatory behavior of buoyant plumes of helium and helium-air mixtures. *Phys. Fluids*, 8:2974–84, 1996.

[2] B. M. Cetegen. Behavior of naturally unstable and periodically forced axisymmetric buoyant plumes of helium and helium-air mixtures. *Phys. Fluids*, 9(12):3742–52, 1997.

[3] A. F. Ghoniem, I. Lakkis, and M. Soteriou. Numerical simulation of the dynamics of large fire plumes and the phenomenon of puffing. *Symposium (International) on Combustion*, 26(1):1531 – 1539, 1996.

[4] X. Jiang and K.H. Luo. Direct numerical simulation of the puffing phenomenon of an axisymmetric thermal plume. *Theor. Comp. Fluid Dyn.*, 14:55–74, 2000.

[5] B. M. Cetegen, Y. Dong, and M. C. Soteriou. Experiments on stability and oscillatory behavior of planar buoyant plumes. *Phys. Fluids*, 10(7):1658–65, 1998.

[6] M. C. Soteriou, Y. Dong, and B. M. Cetegen. Lagrangian simulation of the unsteady near field dynamics of planar buoyant plumes. *Phys. Fluids*, 14(9):3118–40, 2002.

[7] F. Plourde, M. V. Pham, S. D. Kim, and S. Balachandar. Direct numerical simulations of a rapidly expanding thermal plume: structure and entrainment interaction. *J. Fluid Mech.*, 604:99–123, 2008.

[8] T. Hattori, N. Bartos, S. E. Norris, M. P. Kirkpatrick, and S. W. Armfield. Experimental and numerical investigations of the unsteady behaviour for the near-field pure plume flow. *Exp. Therm. Fluid. Sci.*, submitted.

[9] T. Hattori, S. W. Armfield, and M. P. Kirkpatrick. Transitional ventilated filling box flow with a line heat source. *Int. J. Heat Mass Transfer*, 55(13–14):3650–65, 2012.

[10] S. W. Armfield and R. Street. An analysis and comparison of the time accuracy of fractional-step methods for the Navier-Stokes equations on staggered grids. *Int. J. Numer. Methods Fluids*, 38(3):255–82, 2002.

[11] S. W. Armfield. Ellipticity, accuracy, and convergence of the discrete Navier-Stokes equations. *J. Comput. Phys.*, 114(2):176–84, 1994.

[12] C. M. Rhie and W. L. Chow. Numerical study of the turbulent-flow past an airfoil with trailing edge separation. *AIAA Journal*, 21(11):1525–1532, 1983.

[13] B. P. Leonard and S. Mokhtari. Beyond first-order upwinding: The ultra-sharp alternative for non-oscillatory steady-state simulation of convection. *Int. J. Numer. Methods Eng.*, 30(4):729–66, 1990.

[14] H. L. Stone. Iterative solution of implicit approximations of multidimensional partial differential equations. *SIAM Journal on Numerical Analysis*, 5(3):pp. 530–58, 1968.

[15] H. A. van der Vorst. Iterative solution methods for certain sparse linear systems with a non-symmetric matrix arising from PDE-problems. *J. Comput. Phys.*, 44:1–19, 1981.

[16] T. Fujii. Theory of the steady laminar natural convectiol above a horizontal line heat source and a point heat source. *Int. J. Heat Mass Transfer*, 6(7):597–606, 1963.